TU Delft

Delft University of Technology

Organocatalyst reactivation with improved performance in O_2-mediated styrene synthesis

Mercadal, Juan J.; Osadchii, Dmitrii; Zarubina, Valeriya; Valero-Romero, María José; Melián-Cabrera, Ignacio

DOI
10.1016/j.mcat.2022.112525

Publication date
2022

Document Version
Final published version

Published in
Molecular Catalysis

Citation (APA)
Mercadal, J. J., Osadchii, D., Zarubina, V., Valero-Romero, M. J., & Melián-Cabrera, I. (2022). Organocatalyst reactivation with improved performance in O_2-mediated styrene synthesis. *Molecular Catalysis*, *529*, Article 112525. https://doi.org/10.1016/j.mcat.2022.112525

Important note
To cite this publication, please use the final published version (if applicable).
Please check the document version above.

Copyright
Other than for strictly personal use, it is not permitted to download, forward or distribute the text or part of it, without the consent of the author(s) and/or copyright holder(s), unless the work is under an open content license such as Creative Commons.

Takedown policy
Please contact us and provide details if you believe this document breaches copyrights.
We will remove access to the work immediately and investigate your claim.

This work is downloaded from Delft University of Technology.
For technical reasons the number of authors shown on this cover page is limited to a maximum of 10.

Molecular Catalysis 529 (2022) 112525

Contents lists available at ScienceDirect

Molecular Catalysis

journal homepage: www.journals.elsevier.com/molecular-catalysis

Organocatalyst reactivation with improved performance in O_2-mediated styrene synthesis

Juan J. Mercadal [a], Dmitrii Osadchii [b], Valeriya Zarubina [a,c], María José Valero-Romero [d], Ignacio Melián-Cabrera [a,e,*]

[a] Faculty of Science and Engineering, University of Groningen, Nijenborgh 4, Groningen 9747 AG, the Netherlands
[b] Catalysis Engineering, Chemical Engineering Department, Faculty of Applied Sciences, Delft University of Technology, Van der Maasweg 9 HZ, Delft 2629, the Netherlands
[c] Erasmus University College (EUC), Erasmus University Rotterdam, Nieuwemarkt 1A HP, Rotterdam 3011, the Netherlands
[d] Departamento de Ingeniería Química, Andalucía Tech, Universidad de Málaga, Campus de Teatinos s/n, Málaga 29071, Spain
[e] Applied Photochemistry and Materials for Energy Group, University of La Laguna, Avda. Astrofísico Francisco Sánchez, s/n, PO BOX 456, San Cristóbal de La Laguna, S/C de Tenerife 38200, Spain

ARTICLE INFO

Keywords:
Organocatalysis
Catalyst reactivation/regeneration/rejuvenation
MWCNT
Styrene synthesis
Selectivity-induced conversion model

ABSTRACT

An *in situ* thermal reactivation of a multi-walled carbon-nanostructure (MWCNT) is feasible with improved performance in the O_2-mediated styrene synthesis, also called oxidative dehydrogenation of ethylbenzene (EB). The actual catalyst is the coke deposited at the beginning of the reaction on the MWCNT, denoted as ODH-coke, i.e., forming a supported organocatalyst. The deactivation mechanism is the continuing and severe coking that reduces the surface area and eventually plugs the catalyst bed. The reactivation was carried out *in situ* after studying the combustion kinetics of the ODH-coke, which combusts at lower temperature than the MWCNT. The reactivation generated a different catalyst than the original, formed by porous ODH-coke, unmodified ODH-coke and the MWCNT backbone. The performance of such reactivated organocatalyst was improved, becoming more selective to styrene and less to CO_x. This was explained by the increased concentration of ketonic and phenol groups, during the reactivation. Explaining the conversion enhancement is not straightforward because the reaction is limited in O_2. For this, a model was applied that explains that the increased EB conversion is caused by the lowered CO_x selectivity. The model also explains the EB conversion decay with time on stream, due to the enhanced CO_x selectivity; though the nature of the latter effect is not yet fully understood. This work brings three main messages: (a) survival of the MWCNT backbone against gasification/combustion, (b) a better organocatalyst is formed after reactivation, and (c) a model which explains the conversion-selectivity changes (improvement and decay). The latter represents a change in paradigm since conversion and selectivity are considered independent parameters, in heterogeneous catalysis.

1. Introduction

A few required transformations to achieve sustainable development goals have been debated [1], among which a more sustainable industry was considered. This can include optimizing resources across the chemical value chain and enabling a circular, waste-free chemical industry [2]. In this direction, making use of earth-abundant resources is an attractive option since technologies would be more scalable. Elemental carbon precursors can suit that role. For instance, carbon nanotubes are being used in various high-tech applications due to their

Abbreviations: **BET**, Brunauer–Emmett–Teller model; **BJH**, Barrett-Joyner-Halenda model; **CO_x**, it represents the sum of CO and CO_2; **EB**, ethylbenzene; **EB-ODH**, oxidative dehydrogenation of ethylbenzene; **GHSV**, gas hourly space velocity; **MWCNT**, multi-walled carbon nanotube; ***ṅ***, symbol used for molar flowrate; **ODH**, oxidative dehydrogenation; **ODH-coke**, coke produced during the oxidative dehydrogenation of ethylbenzene; **PSD**, pore size distribution; ***S***, symbol used for selectivity; **ST**, styrene; **TPO**, temperature-programmed oxidation; **WHSV**, weight hourly space velocity; ***X***, symbol used for conversion; **XPS**, X-ray photoelectron spectroscopy.

* Corresponding author at: Applied Photochemistry and Materials for Energy Group, University of La Laguna, Avda. Astrofísico Francisco Sánchez, s/n, PO BOX 456, San Cristóbal de La Laguna, S/C de Tenerife 38200, Spain.
E-mail address: ignacio.melian.cabrera@ull.edu.es (I. Melián-Cabrera).

https://doi.org/10.1016/j.mcat.2022.112525
Received 22 June 2022; Received in revised form 14 July 2022; Accepted 18 July 2022
Available online 27 July 2022
2468-8231/© 2022 The Authors. Published by Elsevier B.V. This is an open access article under the CC BY license (http://creativecommons.org/licenses/by/4.0/).

exceptional mechanical, thermal and electrical properties [3]. Implementing such carbon-based materials in catalytic technologies would be a promising route. These processes would depend less on scarce raw materials and, consequently, will become more sustainable [4].

Porous nanostructured carbon materials possess good electron transfer ability, high thermal conductivity, tuneable porosity, chemical stability and tailorable active surface functional groups [5–9]. Notable examples on catalytic applications can be found for pure carbon-based materials [10–13], metal-free carbon-based materials [7,14], coke-coated oxides [15–17], or metal-containing porous carbons [14, 18–20], to cite a few. During the catalytic process, a typical deactivation phenomenon comes from the deposition of organic species, also called fouling, which leads to a depletion of the catalyst porous texture and performance. Reactivation (often also denoted as regeneration or rejuvenation) of carbon-based catalysts after use, due to the organic species deposition, has received hardly any attention in the literature. However, this is fundamental to extend their lifetime. In other words, studying how to reactivate these materials will enable extending their operational lifetime.

A chemical reactivation/regeneration process is one option, but reagents are costly and procedures are often complex to implement. However, thermal oxidative treatments, which uses air/O_2 are simpler and they can be done *in situ* in the reactor, simplifying the process notably. This approach is, however, intrinsically challenging to apply on carbon-based catalytic materials, due to their limited thermal stability, particularly under severe oxidizing conditions. A fouled inorganic-based catalyst is a much easier case as it can be reactivated by air-calcination, e.g. fluid-catalytic cracking catalysts [21]. But such strategy on a fouled carbon-based catalyst or carbon catalyst support is not a rational choice. This is because it would undergo combustion or gasification simultaneously with the organic/coke deposits. It is generally taken for granted that a fouled/coked carbon-based catalyst cannot be regenerated by a thermal oxidative treatment. The present study will show that this is not entirely true. A successful thermal oxidative reactivation depends on the relative combustion kinetics of both species; whether the deposited organic species and the carbon catalyst combustions are thermally resolved at appropriate experimental conditions.

In order to study the carbon-based catalyst regeneration strategy, we chose a reaction of applied relevance: the oxidative dehydrogenation of ethylbenzene into styrene. Styrene (ST) is conventionally obtained at industrial scale by the equilibrium-limited steam-based ethylbenzene (EB) dehydrogenation (Fig. 1(1)), at a large scale world-wide [22]. Conducting the reaction with oxygen/air (denoted as oxidative dehydrogenation, ODH; Fig. 1(2)) has various differences over the conventional dehydrogenation (note: in this work, we will denote the O_2-based ODH as ODH or EB-ODH for simplicity): there are no equilibrium boundaries allowing a complete EB conversion, it works at lower temperatures, it is exothermal and, the EB recycle loop can be avoided [23]. A benefit on energy consumption is a topic of debate since the conventional process produces H_2 and tars, and both can be used in the

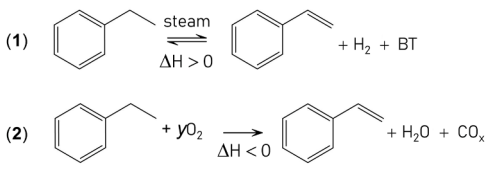

Fig. 1. Alternative ways to produce styrene: (**1**) endothermal steam-assisted dehydrogenation of ethylbenzene (EB), where BT represents benzene and toluene as by-products; (**2**) exothermal oxidative dehydrogenation where CO_x represents CO + CO_2. The amount of required O_2 has been denoted as ***y***. This is 0.5 for the styrene reaction but it is higher for the CO_x forming reactions. See Fig. 2 for more insights on the stoichiometries. The overall ***y***-parameter changes depending on the catalyst and reaction conditions. Under our reaction conditions, O_2 was fully converted.

energy balance [22]. The real benefits of the EB-ODH process are in the higher yield per pass and no compression costs related to EB recycling. There are still some challenges for the EB-ODH process: the oxidant makes the reaction harsher for the catalyst, CO/CO_2 (CO plus CO_2 is denoted as CO_x) are co-produced that have no value and, coke (denoted as ODH-coke) is vastly deposited causing deactivation [24]. The extensive coke deposition and relevance of the reaction made this case attractive for us to study. It should be mentioned that this reaction has not been implemented due to selectivity and stability (or catalyst reactivation) issues.

Carbon-based catalysts are active for this reaction, such as activated carbons [25,26], onion-like structures [27,28], nanofibers [29,30], nano-diamonds [28,31], hierarchical porous carbons [32–34] and multi-walled carbon nanotubes (MWCNT) [24,35,36]. There exist more catalyst types for this reaction but are not mentioned as it is out of the scope of this work. For this work, we employed a MWCNT as model catalyst as it is a competitive system under industrially-relevant reaction conditions [24].

Many studies on this reaction have applied a high O_2/EB ratio (≥ 1). However, these conditions are not industrially relevant. This is because at such a high O_2/EB ratio, unconverted O_2 downstream the reactor would enter into the distillation section causing explosive conditions. This is the reason why we carefully set reaction conditions where O_2 is fully converted. This can be achieved by using: (1) a O_2/EB ratio slightly higher than the stoichiometric ratio for the ST reaction (0.6 versus the stoichiometric of 0.5) and (2) a reaction temperature at which O_2 is fully converted. Another important aspect is using a high EB concentration, e.g. 10 vol.%, which is a requirement for industrial operation, while previous reported studies operated at diluted EB concentrations (typically 0.3 to 2.9 vol.%). Table S1 provides some literature examples with their applied reaction conditions, featuring low EB concentration and an O_2 excess which are not practical conditions for the reasons outlined above. In summary, our chosen reaction conditions were set to be industrially relevant. A consequence of that is a severe ODH-coke deposition. A situation that requires catalyst reactivation. In this work, we employed the term ´reactivation´ that is usually the same as ´regeneration´. But there is a subtle difference here; the reactivated catalyst still contains some residual ODH-coke, whereas a regeneration would imply the full removal of the ODH-coke.

Note that the catalyst performance can be optimized under low O_2 partial pressure by staging it across the reactor [37]. This is beneficial to have a high selectivity, high conversion and lower coking. However, coking is still present and reactivation will be required at a certain time.

It should be mentioned that the actual catalyst is the ODH-coke deposited on the MWCNT at the beginning of the reaction, forming a kind of supported organocatalyst. Hence, it is not a carbocatalysis concept involving a carbon material but an organocatalysis concept involving the ODH-coke. Initially, the MWCNTs C=O groups play a role as initiators. Thus, the MWCNT acts as initiator of the ODH-coke and then fulfils the role of a support (eventually, the MeO_x residue can also have a role in the reaction but this is not known to date). The active ODH-coke has been reported for aluminas, P-silicas, MWCNT and C/silica hybrids at similar reaction conditions [15,16,24,37–40]. This was also proven by others at different reaction conditions [41,42]. Its composition and structure have been elucidated in various studies; it comprises carbon, oxygen and hydrogen forming a system of condensed aromatic rings with conjugated double bonds containing C=O functional groups [15,41,42]. The primary deactivation mechanism in our case is the over-coking which reduces the textural parameters and the catalyst bed is eventually plugged, leading to run-away/explosive conditions. In other words, the ODH-coke is the catalyst but too much of it becomes a deactivating agent. As it will be shown, the thermal oxidative reactivation of an ODH-fouled MWCNT is viable with improved performance. The latter was a surprising outcome where some explanations are provided based on catalyst characterization and model-based calculations.

2. Experimental and theoretical methods

2.1. Materials

The purified MWCNT was provided by Hyperion (CS-02C-063-XD). The extrudates were crushed and sieved into a 212–425 μm fraction and this fraction was used for the catalytic tests, reactivation and characterization studies. Anhydrous ethylbenzene (99.8%) was purchased from Sigma-Aldrich, as well as all the products for calibrating the gas chromatograph. All gases employed in this study were of analytical 5.0 grade, ca. 99.999% purity. The materials investigated in this study are summarized in Table 1.

2.2. Catalyst characterization methods

Thermogravimetric analysis (TGA) was carried out in a SDTA851e Mettler-Toledo analyzer. The weight loss was monitored for a temperature program starting from 30 to 700 °C with a heating rate of 3 °C/min using a 100 mL/min NTP flow of synthetic air. Blank curve subtraction using an empty crucible was used to eliminate crucible effects upon heating. The oxidation rate patterns (TPO) were derived from the TGA derivative profiles. The oxidation rate is given as $-d\alpha/dT$ where $\alpha = (W/W_o \times 100)$, W_o is the initial weight and W the weight at each temperature. Nitrogen physisorption analyses were measured at −196 °C on a Micromeritics ASAP 2420. Fresh and reactivated samples were degassed at 200 °C for 10 h under vacuum. Spent samples were degassed at 150 °C for 10 h to ensure that the coke deposited on the MWCNT was not altered during the degassing. The surface area was calculated with the standard BET method (S_{BET}) and was termed as 'BET area' following the recommendations by Thommes et al. [43]. The pore volume (V_T) was calculated using the single point at the relative pressure of 0.98 in the desorption branch [44]. An accurate assessment of the mesopore size distributions were obtained using the Barrett, Joyner and Halenda (BJH) model applied to the N_2 adsorption data to avoid pore network effects, for comparative purposes among the materials. The micropore volume (V_{micro}) was determined by the *t*-plot method. The parameter $V_{meso/macro}$ includes mainly mesoporosity but also some macroporosity; the macroporosity is the one detected by this technique for pores above 50 nm. Nitrogen as probe molecule in gas adsorption analysis can have limitations when assessing micropores-containing materials. Therefore, care was taken in choosing an appropriate equilibration time, during the measurements, to avoid mass transfer limitations associated to the micropores.

XPS measurements were performed on a K-alpha Thermo Fisher Scientific spectrometer using a monochromatic Al Kα X-ray source. The measurements were performed at ambient temperature, and the chamber pressure during the measurements was about 10^{-7} mbar. A flood gun was used for charge compensation. Each sample was measured in at least five different points. The spectra were analyzed using the Thermo Avantage software package. Background subtraction was done using the setting "SMART". All spectra were calibrated by setting the binding energy of the main C*1s* peak at the reference value of 284.4 eV (not shown). Deconvolution of the O*1s* spectra was performed using a mixed Gauss-Lorentz function, where the Lorentzian contribution was set to 30%. The quantification was done using the Scofield sensitivity factors [45]. Difference in depth of analysis for different photoelectron lines was accounted for by using the TPP-2M method. This allows to calculate the surface elemental composition. Then, by deconvoluting the O*1s* lines into components, the atomic surface percentages for the different surface groups were calculated.

2.3. Catalytic activity measurements

The catalytic tests were performed in an EFFI® micro activity setup having a quartz fixed bed reactor (inner diameter 10.2 mm) in a downflow operation. The reaction conditions were industrially relevant, meaning a high EB concentration (ca. 10 *vol.*%) and limited O_2, to avoid explosive conditions if O_2 would be present downstream the reactor. The reactor was loaded from top to bottom with a quartz wool plug, the catalyst bed, and another quartz wool plug. The catalyst bed height was ca. 30 mm (2.4 ml, 0.585 g) of fresh MWCNT (212–425 μm). The reactor gas feed consisted of a mixture of nitrogen, synthetic air, and ethylbenzene vapor. In order to create such a feed stream, a liquid ethylbenzene flow of 3 g/h was evaporated (10.61 ml/min vapor at STP) and mixed with a stream of N_2 and air. The flows were set in such a way to give a gas feed with a total flowrate of 108 ml/min (STP) at a concentration of ca. 10 vol.% of ethylbenzene. The catalytic test with the 15h-reactivated MWCNT was done using a 0.8 ml catalyst bed volume (bed height of ca. 10 mm, 0.335 g). The reactor gas feed was adjusted to keep the same volumetric space velocity: i.e., a liquid ethylbenzene flow of 1 g/h was evaporated (3.54 ml/min vapor at STP) and mixed with a stream of N_2 and air. The flows were set to give a gas feed with a total flowrate of 36 ml/min (STP) at a concentration of ca. 10 vol.% of ethylbenzene. The runs were carried out in cycles of 40 h in total with alternating steps of 15 h and 4 h with O_2/EB ratio of 0.6 and 0.2, respectively, and temperatures of 475 and 450 °C. These O_2/EB ratios determined the relative flow rates of nitrogen and air in the gas feed stream. The gas hourly space velocity (GHSV) was kept constant in both runs: for the fresh MWCNT run it was (6480 ml/h)/(2.4 ml) = 2700 l/l/h and for the 15h-reactivated material it was (2160 ml/h)/(0.8 ml) = 2700 l/l/h. The pressure in the reactor varied in the range of 1.8–2.2 bar. The reactor outlet flow was analyzed using an online two-channel gas chromatograph with TCD and FID detection and a combination of columns (0.3 m Hayesep Q 80-100 mesh with back-flush, 25 m × 0.53 mm Porabond Q, 15 m × 0.53 mm molsieve 5 Å and 30 m × 0.53 mm RTX-1). Such a configuration allowed detection and quantification of permanent gases (CO_2, H_2, N_2, O_2, CO) and hydrocarbons (methane, ethane, ethene, benzene, toluene, ethylbenzene, styrene, and heavy aromatics). The oxygen conversion was 100%, unless otherwise stated. The characterizations of the after-reaction catalysts were done after the complete testing cycle. The conversion and selectivities are defined as:

$$X_{EB} = \frac{[\dot{n}EB]_{IN} - [\dot{n}EB]_{OUT}}{[\dot{n}EB]_{IN}} \times 100 \quad (1)$$

and,

$$S_{Product\ X} = \frac{\dot{n}Product\ X}{[\dot{n}EB]_{IN} - [\dot{n}EB]_{OUT}} \times 100 \quad (2)$$

Table 1
List of the materials and treatments investigated in this work.

Material	Nature	Treatment
Fresh MWCNT	As-received	None, commercial material
After reaction	Spent catalyst	After reaction according to the described reaction program
Reactivation 5 h	Reactivated	*In situ* reactivation, 1% O_2/Ar, 450 °C,[a] 5 h
Reactivation 10 h	Reactivated	*In situ* reactivation, 1% O_2/Ar, 450 °C,[a] two steps of 5 h (10 h)
Reactivation 15 h	Reactivated	*In situ* reactivation, 1% O_2/Ar, 450 °C,[a] three steps of 5 h (15 h)

[a] Heating program: room temperature up to 450 °C at 3 °C/min.

Where $\dot{n}$-values are the molar flowrates.

2.4. Catalyst reactivation methodology

The *in situ* reactivation method was carried out in the EFFI® micro activity setup, after the reaction. For this, the EB feed was switched off at the temperature of 450 °C and the sample was firstly exposed to a N_2 flow to clean the catalyst surface from weakly physisorbed EB and reaction products. Secondly, the temperature was lowered to room temperature. The reactor was opened and part of the catalyst was recovered for characterization as follows. The after-reaction catalyst was entirely unloaded, thoroughly mixed and a certain amount was taken for analysis (ca. 20 mg for TGA/TPO and 50–100 mg for physisorption). After this step, the material was loaded back to the reactor, purged with N_2 and then it was exposed to a synthetic mixture of 1% vol. O_2/Ar with a flowrate of 100 ml/min STP. The temperature was raised from room temperature up to 450 °C at 3 °C/min and held for 5 h. Subsequently, the gas flow was changed to N_2 to stop the reactivation and the temperature was decreased to ambient temperature. Up to three reactivation steps in total on the same sample were carried out. Each one consisted of a ramp at 3 °C/min with an isotherm at 450 °C for 5 h. After each step, some material was taken for characterization at room temperature following the same protocol as explained above for the after-reaction catalyst. The materials are denoted as 'Reactivation *x* h', where *x* denotes the total treatment time in hours at the reactivation temperature of 450 °C (i.e., *x* = 5, 10 or 15 h). The catalytic test of the reactivated material was done on the material that underwent three reactivation steps of 5 h, i.e., Reactivation 15 h, as this was the optimal case in terms of ODH-coke removal for the studied conditions. Note that this reactivation time is a relative optimum since the absolute optimum is yet to be determined.

2.5. Theoretical model

A model was applied by setting an O_2 balance across the reactor. It assumes that O_2 is fully consumed, which was confirmed experimentally. The O_2 mass balance across the reactor when O_2 is fully consumed by reactions R1, R2 and R3 is given as:

$$[\dot{n}O_2]_{IN} = \left[\dot{n}O_2^{R_1} + \dot{n}O_2^{R_2} + \dot{n}O_2^{R_3}\right]_{consumed} \quad (3)$$

where the $\dot{n}$-values are the molar flowrates, the subscript IN means fed in the reactor, and the superscripts indicate the reaction (Fig. 2). The reaction was carried out at this condition:

$$[\dot{n}O_2]_{IN}/[\dot{n}EB]_{IN} = 0.6 \quad (4)$$

Considering the stoichiometric relations for the three reactions Fig. 2), the following expression for the EB conversion can be obtained from ((3) and (4):

$$X_{EB}(\%) = \frac{[\dot{n}O_2]_{IN}/[\dot{n}EB]_{IN}\cdot 10^4}{\frac{1}{2}S_{ST} + \frac{13}{2}S_{CO} + \frac{21}{2}S_{CO_2}} = \frac{6000}{\frac{1}{2}S_{ST} + \frac{13}{2}S_{CO} + \frac{21}{2}S_{CO_2}} \quad (5)$$

where S_{ST} is the selectivity to styrene; S_{CO} the selectivity to CO and S_{CO_2} the selectivity to CO_2 and all sum 100%.

$$C_8H_{10} + \frac{1}{2}O_2 \rightarrow C_8H_8 + H_2O \quad R1$$

$$C_8H_{10} + \frac{13}{2}O_2 \rightarrow 8CO + 5H_2O \quad R2$$

$$C_8H_{10} + \frac{21}{2}O_2 \rightarrow 8CO_2 + 5H_2O \quad R3$$

Fig. 2. Main macroscopic reactions occurring during the ethylbenzene oxidative dehydrogenation. Main (R1) yielding styrene, and side reactions (R2 and R3) yielding CO and CO_2, respectively. ODH-coke formation is not considered in the model since it represents a small fraction of the fed ethylbenzene.

However, O_2 can also be consumed into undetected compounds. One route is the formation of the ODH-coke (which contains oxygen), but this generally represents a small fraction in the whole run. The reaction also produces tars that condensate in the outlet lines/condenser and are not easy to be quantified. These tars certainly contain oxygen. Therefore, using the O_2/EB in the feed will not represent the O_2 conversion into detected reactions. A more accurate approach would be considering the O_2/EB determined from an experimentally-determined mass balance. Therefore, Eq. (5) can be set more accurately as:

$$X_{EB}(\%) = \frac{([\dot{n}O_2]/[\dot{n}EB])_{IN}^{mass\ balance}\cdot 10^4}{\frac{1}{2}S_{ST} + \frac{13}{2}S_{CO} + \frac{21}{2}S_{CO_2}} \quad (6)$$

Where $([\dot{n}O_2]/[\dot{n}EB])_{IN}^{mass\ balance}$ can be determined by a mass balance of the detected compounds.

The model equation can be expressed as:

$$X_{EB}(\%) = \frac{([\dot{n}O_2]/[\dot{n}EB])_{IN}^{mass\ balance}\cdot 10^4}{\frac{1}{2}(100 - S_{CO_x}) + \frac{13}{2}\left(\frac{1}{R+1}S_{CO_x}\right) + \frac{21}{2}\left(\frac{R}{R+1}S_{CO_x}\right)} \quad (7)$$

$$R = \frac{\dot{n}CO_2}{\dot{n}CO} = \frac{S_{CO_2}}{S_{CO}} \quad (8)$$

Where R is an experimental parameter that depends on the catalyst and reaction conditions. For more information about the model, the reader is referred to Melián-Cabrera and Zarubina [46] where it is described in detail. The model predicts that the highest EB conversion is obtained when the CO_x selectivity is lowest for a given $([\dot{n}O_2]/[\dot{n}EB])_{IN}^{mass\ balance}$. The higher the $([\dot{n}O_2]/[\dot{n}EB])_{IN}^{mass\ balance}$, the higher the EB conversion. However, such a value should not be too high otherwise there would be unconverted O_2 downstream the reactor. A situation that is undesirable for the reasons explained before, i.e., O_2 must be fully converted in the reactor.

The model does not require kinetic parameters but the selectivity to each product. A kinetic model is often a matter of debate and brings some errors in the parameter estimation. In this reaction, it is not known whether the CO_x routes are catalysed or not. Therefore, the proposed model overcomes such limitations in existing knowledge.

3. Results and discussion

3.1. Reaction performance of the fresh MWCNT

The catalyst performance parameters of the fresh MWCNT are given in Fig. 3a. The O_2/EB was studied at 0.6 and 0.2; the latter to evaluate the styrene selectivity in a possible O_2 stage-feeding configuration [37], though this topic is not directly addressed in this paper. The MWCNT was readily active and selective. It indicates that the C=O groups on the MWCNT are the initiation active sites, whereas later, the deposited ODH-coke dominates the reaction performance.

The ST selectivity improves by operating at low O_2/EB and a lower temperature, reaching values above 90% with the remaining side products being CO_x. Despite the high ST selectivity, a significant drop in conversion and yield are observed at low O_2/EB (the ST yield can be found in Fig. S1, and will be discussed in more detail later).

The CO_x decreases at lower temperature, likely by favoring the styrene route in a competitive scheme. The better selectivity to styrene at lower temperature (450 vs 475 °C) can be explained by a higher concentration of C=O/C-OH (redox active sites) at lower temperature. Higher temperature would favor the gasification or combustion of these groups in the presence of reaction O_2 and therefore the catalyst becomes less selective to styrene (keep in mind that the reaction uses O_2). The above statement is based on the elemental compositions reported in [42]. They observed a lower concentration of elemental O in the ODH-coke when the reaction was performed at higher temperature (22 versus 12 wt.% at 400 versus 500 °C). Yet CO_x formation is unavoidable under ODH conditions. The CO_x forming pathway has been proposed to

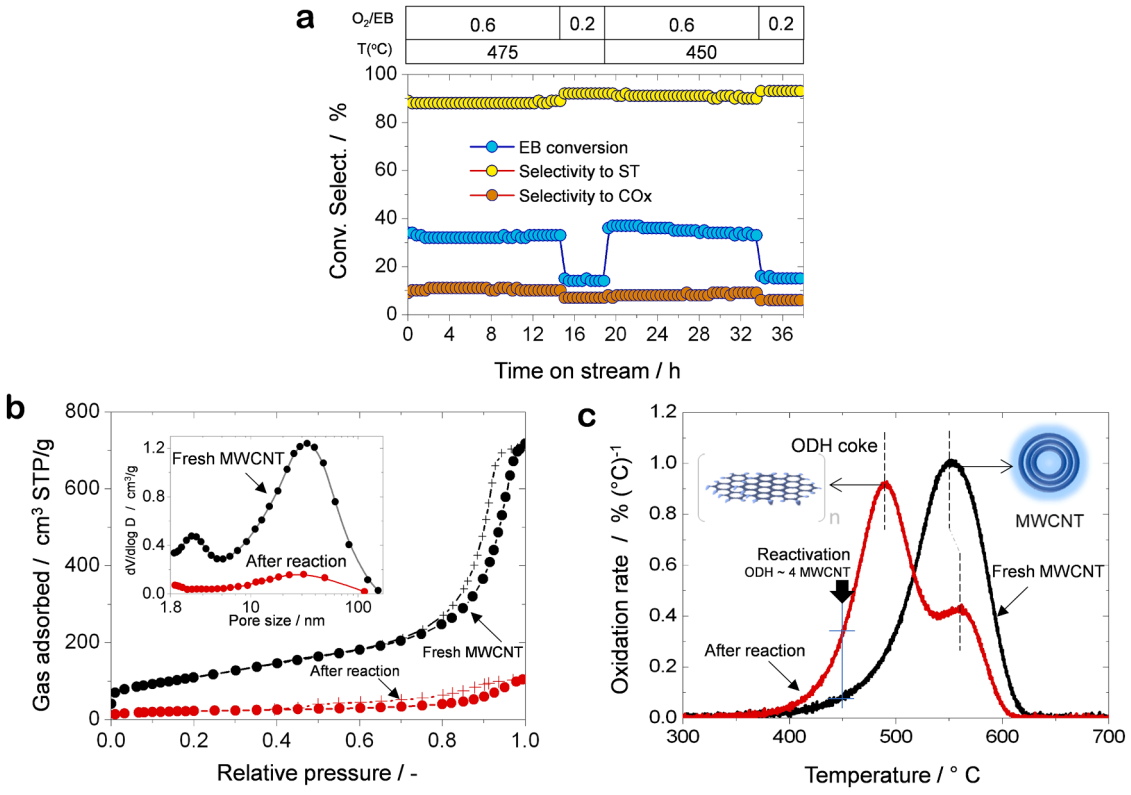

Fig. 3. (**a**) Catalytic performance of the fresh MWCNT in the ethylbenzene oxidative dehydrogenation at various temperatures and O_2/EB ratios as indicated at the top of the graph. The O_2/EB ratios given in the heading correspond to the mass-flow controller values, as an indication. The ones used in the model (later) correspond to the mass-balance values, obtained by gas chromatography together with the reactant and all detected products. (**b**) Nitrogen sorption isotherms at −196 °C for the fresh and after-reaction MWCNT (inset: BJH pore size distribution). (**c**) Conceptual basis of the reactivation strategy shown on the temperature-programmed oxidation (TPO) patterns for the fresh and after-reaction (1st) MWCNT materials.

occur via gasification/oxidation of the deposited ODH-coke [42]. Considering relevant studies on the oxidation stability of CNTs [47,48], CO_x formation could be attributed to the presence of surface defects on the ODH-coke, which would be reactive and prone to gasification/oxidation. In the alkane ODH, it was proposed that CO_x takes place by direct oxidation of the alkane or alkene by oxygen species (O_2^-, O_2^{2-}), which are formed under ODH conditions at defect sites, carboxylic or lactone groups [11,49,50]. However, for the EB-ODH reaction, evidence only exists for CO_x formation via the ODH-coke gasification/oxidation [42]. An area that deserves further investigation to lower this undesirable CO_x route.

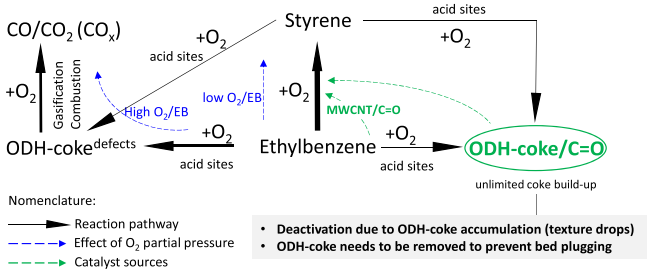

Fig. 4. Reaction pathways during the O_2-based oxidative dehydrogenation of ethylbenzene into styrene and CO/CO_2 (CO_x). The ODH-coke is generated from ethylbenzene or styrene, or both. Ketonic (quinone) groups present on the MWCNT and ODH-coke are considered to be the active sites. CO_x is considered to be formed by oxidation/gasification of the ODH-coke. Here, it is assumed that defects on the ODH-coke are the combustion/gasification sites. This reaction scheme is based on prior knowledge that was recently rationalised in [46]. The effect of O_2/EB on selectivity has been indicated with blue dashed lines. The thickness of the black lines indicates the reaction rates in qualitative terms. The green dashed lines show the various catalyst sources, containing C=O groups, for the EB-to-ST step. The deactivation comes from the accumulation of ODH-coke (i.e., over-coking) that occurs with time on stream leading to a lowering of the textural features and eventually plugging the catalyst bed (For interpretation of the references to color in this figure legend, the reader is referred to the web version of this article.).

Due to the complexity of the reaction and catalyst, Fig. 4 summarizes the reaction pathways during the O_2-based oxidative dehydrogenation of EB. In this system, the complexity comes from the fact that the C=O groups on the MWCNT (initially) and on the ODH-coke (later) act as active sites. The scheme also shows the CO_x-forming route through the ODH-coke. It is worth noting that the ODH-coke deposition is much smaller than the main reactions in Fig. 2. For instance, for the fresh-MWCNT run we observed a weight increase of ca. 80 wt.% due to ODH-coke deposition. This corresponds to ca. 0.5% of the total fed ethylbenzene (or ca. 1% in terms of converted EB). This, as well as the tar formation, are important for the general mass balance. But these factors are not affecting the model since this considers the O_2/EB obtained from an experimentally-determined mass balance, Eq. (7) in Section 2.5. However, such an amount of deposited ODH-coke is important for the catalyst texture as it drops significantly. The caption of Fig. 4 provides additional information about the reactions involved.

There is a separate topic that can have an influence. The metal-based residue in the MWCNT (see TGA in Fig. S2) can also play a role in the CO_x formation, by affecting the ODH-coke defects (as an indirect role) or by participating as active species if the metal-species get exposed to the reactants. The MeO_x residue in nanotubes are normally unavoidable. An acid wash is not effective in lowering its content below a certain threshold and high temperatures are required to remove it fully by evaporation/sublimation, ≥ 1800 °C [51]. Due to the complexity of the purification, we did not address it on this commercial material any

further. The residual MeO_x particles in carbon nanotubes are normally covered by graphitic carbon, but the reaction conditions can uncover them, and then becoming catalytically active. Kiciński and Dyjak [52] reviewed the effects of transition metal impurities on the properties and applications of carbon-based materials. The effect on this reaction was not discussed, likely due to the lack of studies on this matter. In summary, the catalytic effects of metal impurities in the CO_x route for this reaction (direct or indirect effects) are not known to the best of our knowledge, and they cannot be ruled out.

Retaking the discussion of Fig. 3a, the EB conversion did not change much with temperature (450 vs 475 °C). But in fact, the opposite effect to what is expected, was observed; a slightly higher EB conversion at lower temperature. This surprising finding is further explained later in Section 3.7, after introducing the model formulation.

Finally, in parallel to the main and side reactions, ODH-coke deposition takes place, as discussed in the Introduction and in Fig. 4. The ODH-coke deposition was evaluated on this material by characterizing the after-reaction catalyst, which is crucial for defining a suitable reactivation protocol.

3.2. Characterization of the after-reaction catalyst

The discussion of this section is based on N_2 physisorption and temperature-programmed oxidation (TPO). The physisorption data of the native MWCNT shows an isotherm type IV with H1 hysteresis and a bimodal pore size distribution (Fig. 3b); as the isotherm does not level off at high P/P_o, this means that there is an underlaying type II behavior due to unfilled macropores. The lower maximum in the pore size distribution corresponds to the inner nanotube channel whereas the higher maximum to the space between the rods (Fig. 3b, inset). The after-reaction catalyst experienced a remarkable decrease of the adsorption and pore size distribution (Fig. 3b and inset). The BET area decreased from 396 to 82 m^2/g (fresh and after-reaction, Table 2). A similar trend was observed for the pore volume (Table 2).

A mass balance of the catalyst bed revealed a weight increase of ca. 80 wt.% due to ODH-coke deposition during reaction.

Temperature-programmed oxidation (TPO) of the after-reaction catalyst exhibited a new lower-temperature peak due to ODH-coke (Fig. 3c; the fresh MWCNT was added for comparison).

All these experimental data evidence the deposition of significant ODH-coke during the reaction. This was already observed in Zarubina et al. [24] though the effect was scarcely discussed. The ODH-coke deposition is generally attributed to weak acidity of the support [42]. The metal-based residue may also affect the coke deposition if they become accessible to the reactants and possess acidity. So, both effects can play a role; surface acidity of the MWCNT and metal-based residue.

Previous studies have reported deposition of ODH-coke on activated carbons [53], carbon nanofibers [54] and carbon nanotubes [35]. The reported values for the carbon nanotubes [35] were smaller to our data, between ca. 0 to 3.8% weight increase as compared to our 80 wt.%. This can be explained by the different reaction conditions. We employed a higher EB concentration (10 vs 2.3 vol.% in [35]); it is more realistic but promotes more ODH-coke deposition. In addition, less O_2 was used by us (O_2/EB = 0.6 vs 1 in [35]) that probably lowers the gasification/combustion of the ODH-coke into CO_x. Or in other words, a high O_2/EB helps to remove the ODH-coke by gasification/combustion. However, unreacted O_2 downstream the reactor is a major problem for implementation as explained earlier.

Overall, our practical reaction conditions lead to significant ODH-coke deposition. A situation that requires catalyst reactivation. Fig. 4 summarizes graphically the deactivation mechanism due to the accumulation of the ODH-coke in the catalyst bed.

3.3. In situ reactivation

The TPO patterns of fresh and after-reaction catalysts are compared in Fig. 3c. The after-reaction catalyst displays two oxidative processes due to ODH-coke (lower temperature peak) and the MWCNT backbone (higher temperature peak). The difference between both peak maxima is ca. 75 °C at the employed conditions. That means that there is enough thermal resolution between both processes to consider a thermal oxidative catalyst reactivation. We carried out the reactivation at 450 °C where the ODH-coke combustion rate is higher than that of the MWCNT, ratio ca. 4 to 1. This would allow to remove selectively the ODH-coke, though some MWCNT is also burnt (likely the more amorphous domains). The justification of this temperature can be further explained with Fig. 5. The difference of the TPO curves is highest at ca. 490 °C. We chose a lower reactivation temperature (450 °C) to avoid a possible hot-spot during reactivation due to the reaction exothermicity. However, additional optimization would provide a more accurate answer about

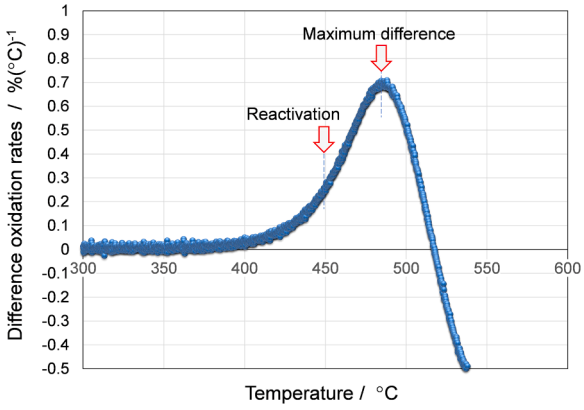

Fig. 5. Difference between the oxidation rate patterns (TPO) of the fresh and after-reaction (1st) MWCNT materials as a function of temperature.

Table 2
Textural properties of the fresh, after reaction and reactivated MWCNT materials.

Material	S_{BET} (m^2/g)	V_T (cm^3/g)	V_{micro} (cm^3/g)[a]	$V_{meso/macro}$ (cm^3/g)[b]
Fresh MWCNT	396	1.039	<0.001	1.039
After reaction (1st)[c]	82	0.157	0.009	0.148
Reactivation 5 h	386	0.358	0.118	0.240
Reactivation 10 h	516	0.459	0.126	0.333
Reactivation 15 h	645	0.610	0.108	0.502
After reaction (2nd)[d]	9	0.026	<0.001	0.026

[a] V_{micro} determined by the Harkins-and-Jura *t*-plot method (error ~0.001 cm^3/g).
[b] $V_{meso/macro} = V_T - V_{micro}$, this parameter involves mostly mesoporosity but also some macroporosity (Fig. 6c).
[c] Spent catalyst after testing the fresh MWCNT.
[d] Spent catalyst after testing the 15h-reactivated catalyst.

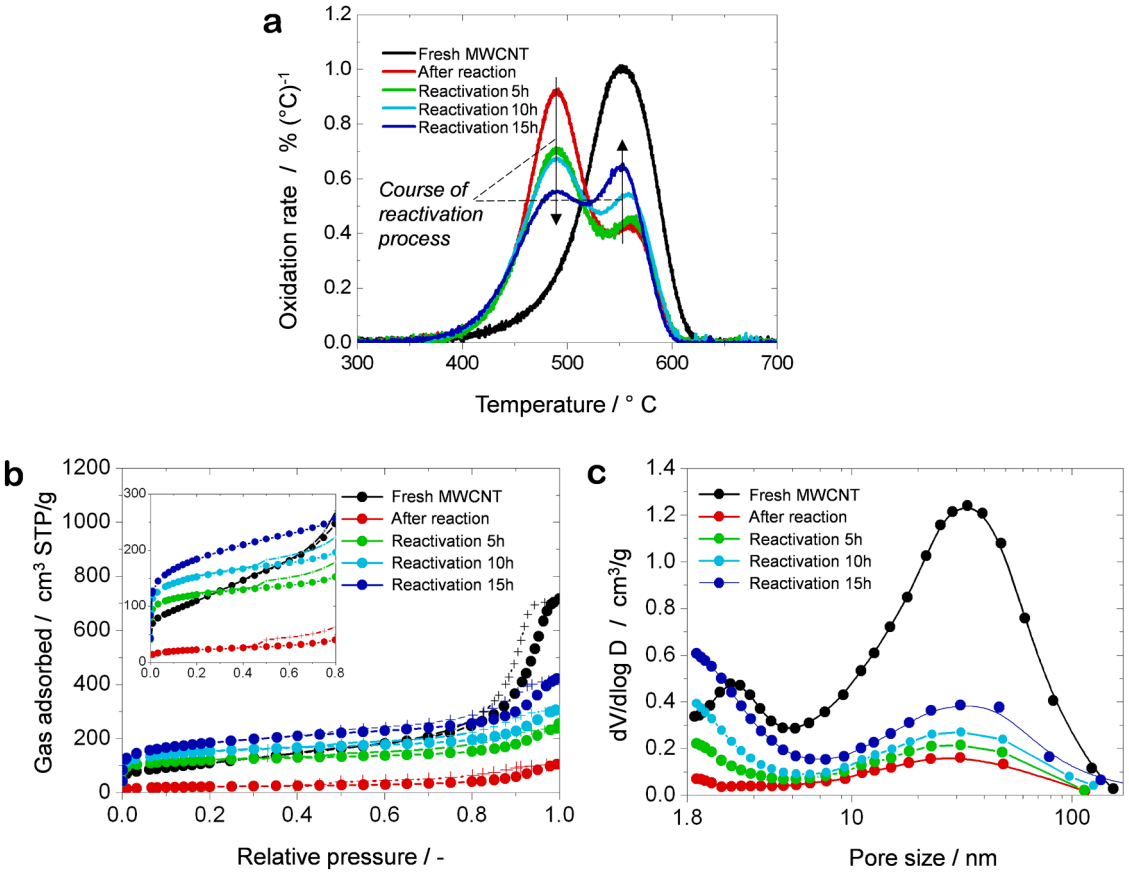

Fig. 6. *In situ* reactivation of a fouled MWCNT (450 °C, 1% vol. O_2/Ar) at various processing times: (**a**) TPO patterns, (**b**) nitrogen sorption isotherms at −196 °C (inset: amplification in the low-relative-pressure region) and (**c**) BJH pore size distributions of the reactivated materials including the fresh and after-reaction (1st) counterparts. Up to three reactivation steps in total on the same sample were carried out, corresponding to the 5h-, 10h- and 15h-reactivated materials.

the best reactivation temperature in terms of ODH-coke removal and catalyst performance. Such an optimization was not carried out in this study. In order to control the combustion exothermicity and avoid a hot-spot and thermal run-away, the reactivation was carried out using a diluted gas stream of 1% vol. O_2/Ar.

3.4. Characterization of the reactivated catalysts

The after-reaction catalyst was reactivated *in situ* at various processing times (5, 10 and 15 h). The resulting materials were characterized by TPO and N_2 gas adsorption-desorption. Fig. 6a displays the TPO profiles for each reactivated sample, which allows for assessing the degree of reactivation in semi-quantitative terms. The arrows in Fig. 6a indicate the course of reactivation. The ODH-coke peak decreases whereas the MWCNT increases due to the ODH-coke removal by gasification/combustion during the reactivation.

A mass balance for each reactivation step shows a ca. 15–20 wt.% decrease due to ODH-coke removal. In particular, 16% for the first, 17% for the second and 24% for the third reactivation (for each reactivation some material was separated for characterization). Considering these partial weight decreases, the total weight of the final 15h-reactivated catalyst can be calculated. It resulted to be slightly below the starting MWCNT (0.570 vs 0.585 g). However, the TPO of the 15h-reactivated material still showed ODH-coke (Fig. 6a). These observations can be justified by the partial burning of the MWCNT (amorphous domains). This is logical since the TPO of the MWCNT was not zero at the reactivation temperature. It represents a trade-off between reusing the catalyst or disposing it off. Extending the reactivation time to remove all the ODH-coke can be done in a follow-up study. However, we found that a partially reactivated one was better than the original (discussed later). Therefore, this should be kept in mind when carrying out the optimization study.

The porosity was evaluated by N_2-physisorption (Fig. 6b and c, Table 2). For all reactivated materials, the isotherms retain the original shape but the adsorption values are different to the fresh MWCNT. The low-relative-pressure region raises steeper (inset in Fig. 6b) whereas the high-relative-pressure zone sits lower than the fresh MWCNT. These imply that the surface areas are higher and the pore volumes are lower (Table 2). The BET areas increase significantly (396 m^2/g for the fresh versus 386, 516 and 645 m^2/g for 5, 10 and 15 h reactivation times). Changes in the pore size distributions (PSD) are shown in Fig. 6c. New and smaller pores were formed, increasing their contribution with the reactivation time. Micropores were quantified by the *t*-plot method (Table 2). The micropore volumes for the reactivated materials were high and nearly constant, while the mesopore/macropore volumes increased with the reactivation time, as compared to the after-reaction catalyst (1st). These values, in addition to the PSD trends, indicate a shift of the porous texture towards smaller pore sizes as a consequence of a favored ODH-coke gasification/combustion with time. The macroporosity of the reactivated materials is much smaller than the fresh MWCNT (Fig. 6c). Compared to the fresh MWCNT, the increased BET areas for the reactivated materials are attributed to both newly-formed micropores and smaller mesopores.

Based on TPO and gas adsorption, the resulting material (15h-reactivated) still contains ODH-coke displaying micropores and smaller mesopores, with a higher BET area and smaller pore volume than the original MWCNT. It is hypothesized that the new porosity development mainly takes place on the ODH-coke domains. It is unlikely that the MWCNT backbone develops porosity itself, due to breaking of the tubes, since its TPO process takes place at higher temperature (ca. 550 °C). But

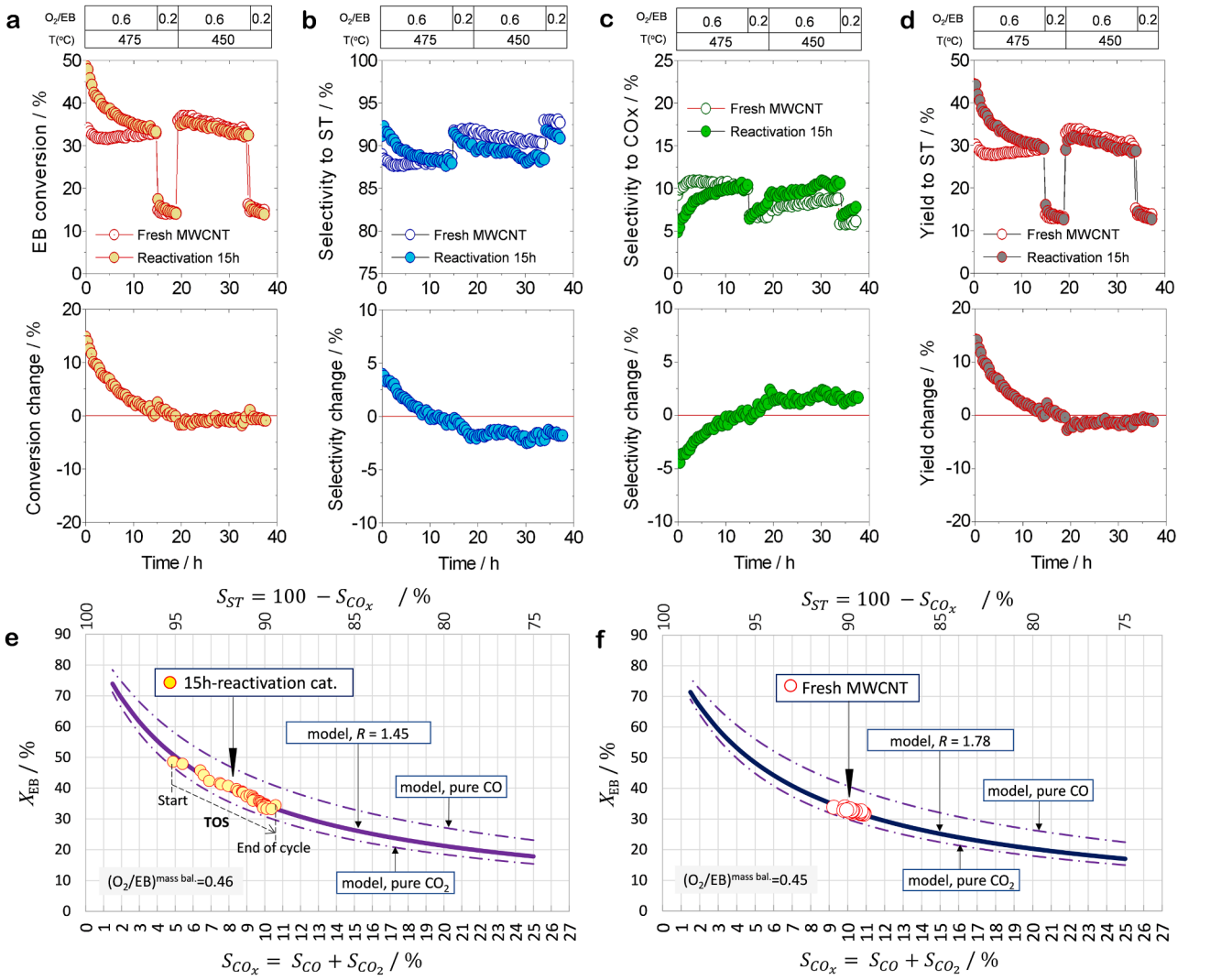

Fig. 7. Catalyst performance parameters as a function of time on stream for the fresh and 15h-reactivated MWCNT in the ethylbenzene oxidative dehydrogenation: (**a**) ethylbenzene conversion; (**b**) selectivity to styrene; (**c**) selectivity to CO/CO_2 (CO_x); (**d**) yield to styrene at various temperatures (475 and 450 °C) and O_2/EB = 0.6 and 0.2 (vol.); GHSV of 2700 l/h/l; 10 vol.% EB. The graphs at the bottom are the difference between the 15h-reactivated catalyst and the fresh MWCNT. Model representation of the EB conversion (X_{EB}) as a function of S_{COx}, including experimental data points of the first step of the catalytic test (475 °C, O_2/EB = 0.6) for: (**e**) 15h-reactivated catalyst and (**f**) MWCNT catalyst. Figs. S3 and S4 provide information about the model for the second and third steps of the test. The O_2/EB ratios given in the headings (**a-d**) correspond to the mass-flow controller values, as an indication. The ones used in the model (**e,f**) correspond to the mass-balance values, obtained by gas chromatography together with the reactant and all detected products.

it cannot be categorically excluded to occur as well due to local hot spots. Based on the position of the main pores at 30 nm (Fig. 6c), which does not change upon reactivation, the breaking of MWCNT tubes does not seem to happen at a detectable level. In other words, if the MWCNTs are broken and shortened, the PSD maximum should be shifted towards lower pore sizes due to the smaller space between the nanotubes. But the amorphous domains present in the MWCNT can develop some porosity as well (the asymmetry and shoulder at lower temperatures of the MWCNTs TPO is indicative of amorphous domains, Fig. 3c or Fig. 6a). Hence, the most plausible phenomenon occurring during the reactivation is the formation of an organocatalyst containing porous ODH-coke, unmodified ODH-coke and the MWCNT (backbone and partially combusted amorphous domains, eventually containing some porosity).

3.5. Reaction performance of the reactivated catalyst

The *in situ* 15h-reactivated material looks promising in view of the removed ODH-coke and textural features. Note that further optimization appears to be possible, and this can be the scope of a separate study. The 15h-reactivated material was evaluated in the reaction and the results were compared to the fresh counterpart in Fig. 7a–d. The bottom of the graphs displays the difference between fresh and reactivated catalysts for an easier comparison. The EB conversion (Fig. 7a) was initially enhanced in ca. 15%, then it decreased and came to a similar level for both catalysts. The ST selectivity was initially higher (Fig. 7b) and the CO_x was smaller (Fig. 7c). These are very positive features since CO_x are unwanted side products. Later in the run, the ST selectivity lowers (CO_x rises) and is ascribed to coking-related effects. When assessing the ST yield (Fig. 7d), a clear benefit of the reactivation is observed for at least 20 h of operation, and afterwards on an equal level for ca. 40 h in total (Fig. 7d-bottom shows this effect clearer). Obtaining an equal yield is already a positive result for the reactivation, but for the initial 20 h-period it was even better than the original catalyst.

It must be kept in mind along the discussion that the selectivities to ST and CO_x sum up to 100% as competitive routes. Consequently, the modification of one leads to a change towards the other. That is, if the ST selectivity increases by x%, the CO_x selectivity decreases x%, and vice versa.

The enhanced EB conversion can have several causes, but the most convincing explanation is found in the selectivity. The reaction runs at 100% O_2 conversion, and a lowering in the CO_x selectivity can liberate O_2 for the main reaction, because the reactions involving CO and CO_2 consume more O_2 than the main one (see stoichiometry of the reactions in Fig. 2). A phenomenological model was applied to develop a better understanding on this matter. It assumes full oxygen conversion (that occurs in practice) where the EB conversion can be expressed as a function of the selectivity to CO_x (see model description in Section 2.5). In a system of competing reactions having a limiting reactant (this case O_2), the conversion of the other reactant (this case EB) is not an independent variable but is dependent on the selectivities. This constitutes the basis of our model and is exactly what we observed when adding the experimental data into the model curves (Fig. 7e and f); a very good match. The model also works for the other conditions of the catalytic run for both catalysts (Figs. S3 and S4). Hence, the model explains that the EB conversion rise at the beginning is the consequence of the catalyst being more selective to styrene after reactivation (or less to CO_x). Moreover, the model explains the drop in EB conversion with time on stream (TOS) of the reactivated catalyst, since the data fit the model in Fig. 7e. The drop in EB conversion is ascribed to the reduced selectivity to styrene (or enhanced to CO_x) with TOS. In other words, as the catalyst becomes more selective to CO_x, the EB conversion decreases. This finding is important because instead of having two root-problems (conversion and selectivity), the main problem seems to be the ST selectivity that drops with TOS, or the increased CO_x with TOS (as both CO_x and ST sum up to 100%). The reason for such a selectivity decay is not fully clear to us, though it may be related to changes in the ODH-coke nature, reduced porosity that brings side effects, other unknown effects, or a combination of effects.

Another possible reason for the initial EB conversion increase, can be found in the catalyst density. The density changes upon reactivation and the catalyst becomes denser. The tests for both catalysts were carried out by keeping the parameter $(g_{EB}/h)/(cm^3_{cat}) = 1.25$ fixed, i.e., the same catalyst volume sees the same feed rate, mimicking a constant-volume reactor operation. As the catalyst density increases, it implies that the weight-based parameter $(g_{EB}/h)/(g_{cat})$ is smaller; 5.1 versus 3.0 for the fresh and reactivated catalysts respectively. Therefore, there is more catalyst amount per feed rate. It is a lower WHSV operation and it might explain the enhanced conversion. However, it must be kept in mind that the reaction is limited in O_2, which was 100% converted even at 450 °C. Therefore, it is unlikely that having more catalyst (i.e., more active sites) per EB feed rate would enhance the EB conversion, since O_2 is the limiting reagent.

Another possible interpretation to the enhanced EB conversion would be using the surface areas. The reactivated catalyst displayed a higher BET area and there should be more exposed active sites. However, the surface areas should be normalized to the bed and to the feedstock rate. Calculation of this parameter, $\frac{m^2/bed}{g_{EB}/h}$, leads to a figure of 77 for the fresh MWCNT and 216 for the reactivated catalyst. This indicates that the surface area available at equal feed rate is higher for the reactivated catalyst. However, this cannot explain the higher EB conversion since the reaction is limited in O_2.

The first hypothesis verified by the model, i.e., change in selectivity to CO_x and making O_2 available for the main reaction, seems to be more sensible. This is further supported by recent results using the same model [46]. A series of aluminas were calcined before reaction (500–1200 °C) and tested in the same reaction and the same reaction conditions, where the *in situ* formed ODH-coke was the active site. The aluminas treated at higher temperature displayed a higher ST selectivity and EB conversion. Even the catalysts had less surface area after the thermal treatment (absolute and per catalyst bed), the EB conversion was higher than the base catalyst. The higher EB conversion was explained by the lower selectivity to CO_x (or higher to styrene) using the same model as applied it here. Therefore, the selectivity controls this reaction at the applied practical reaction conditions, when O_2 is fully converted.

Overall, the model predicted well the experimental data, and hence such hypothesis is here considered as the most solid to explain the changes upon reactivation. In summary, the model explains: (a) the initially improved parameters for the reactivated catalyst and (b) the course of the reaction with TOS where there is a link between conversion and selectivity, so they are not independent parameters. The latter refers to the reactivated catalyst (Fig. 7e) since the fresh MWCNT did not change much with TOS though the data fit the model as well (Fig. 7f). The model does however not explain why the reactivated catalyst becomes less selective to styrene (or more towards CO_x) with TOS. This matter deserves further investigation.

3.6. Some model considerations

Fig. 7e plots the modeled EB conversion for three cases; when CO_x is pure CO, when CO_x is pure CO_2 and with the experimental ratio $CO_2/CO = R = 1.45$ for this catalyst and experimental conditions. It is reasonable to observe that the lowest EB conversion is obtained with CO_x as pure CO_2 since this reaction consumes most O_2, R3 in Fig. 2. Therefore, the EB conversion is most sensitive to changes in the selectivity to CO_2. The model curve for the experimental $R = 1.45$ lays between the two extreme cases and therefore it is in agreement. Similar observations about the CO_2/CO ratio were found for other reaction conditions (e.g. Fig. 7f) and in the examples discussed in [46].

3.7. Explaining the unexpected temperature effect

As shown in Fig. 3a, the EB conversion shows a slight increment at 450 °C (TOS 19–33 h) comparing with 475 °C (TOS 0–14 h). One would expect an opposite effect, higher EB conversion at higher temperature. This can be explained with the model. At both temperatures, O_2 is fully converted. At lower temperature, the selectivity towards ST is higher and lower towards CO_x. According to the model, a lower CO_x selectivity leads to higher EB conversion. This is shown in Fig. 8 where data for both temperatures are plotted. It shows that the lower the selectivity to CO_x, the higher the EB conversion. The reason for the lower CO_x selectivity at 450 °C is unknown but a suggestion was outlined earlier; at lower reaction temperature, a higher concentration of C=O/C-OH (redox active sites) might be available, so the catalyst is more ST selective. In other words, higher reaction temperature would favor the gasification/combustion of these groups (in the presence of O_2) and

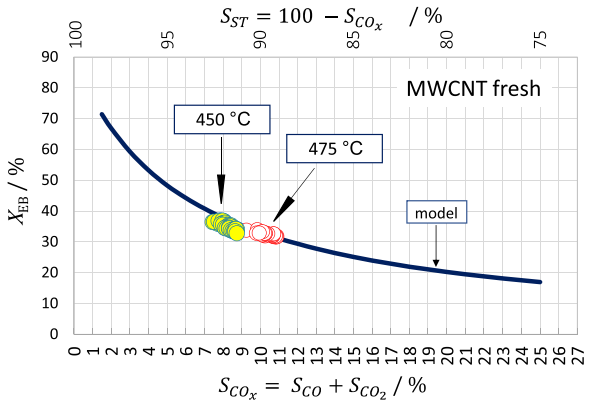

Fig. 8. Effect of temperature on catalyst performance for the fresh MWCNT. Model representation of the EB conversion as a function of S_{COx}, including experimental data points of the first (475 °C, O_2/EB = 0.6) and third (450 °C, O_2/EB = 0.6) steps of the catalytic test for the fresh MWCNT catalyst. Raw data are given in Fig. 3a. For clarity, the model line is an average between both situations, which are very similar to each other. The above O_2/EB ratios correspond to the mass-flow controller values in relation to Fig. 3a.

therefore it becomes less selective to styrene, and more to CO_x. The role of the residual MeO_x should also not be ruled out in the CO_x forming reactions.

3.8. Explaining the lack of conversion decay of the fresh MWCNT

It was shown that there is a significant ODH-coke deposition with a drop of the surface area of the fresh MWCNT catalyst after reaction (396 down to 82 m^2/g). One could wonder why the EB conversion for the fresh MWCNT does not drop with TOS (Fig. 3a), as a consequence of the drop in surface area (i.e., decreasing available active sites). The reason for that is the fact that the reaction is limited in O_2. Therefore, the EB conversion is determined by the selectivity as it was shown with the model. The fact that the selectivity to CO_x does not change much with TOS, it explains the relatively stable EB conversion for the fresh MWCNT. If the O_2/EB ratio would have been set higher (i.e., O_2 conversion $< 100\%$), then it is expected a decay of the EB conversion with TOS due to the over-coking and lowered surface area. However, this condition (higher O_2/EB ratio) was not applied since it is not practical. It can be applied in future studies to confirm the sensitivity of the reaction to the surface areas when O_2 is not limiting, for the sake of completeness.

3.9. Explaining the end-of-the-run pseudo-steady state conversion

In relation to the pseudo-steady state conversion, something similar in terms of the BET area occurs at the end of the runs (Fig. 7a). The EB conversion come very close for both catalysts despite the catalysts have different BET areas (82 versus 9 m^2/g, Table 2). The explanation is found in the selectivity to CO_x, which was very similar for both catalysts at the end of the run, and that determines the EB conversion. As a comparison, the transitional alumina study [15,46], involving aluminas with different surface areas (i.e., 272 to 101 m^2/g or 132 to 58 m^2/bed), showed no relevance of the surface area when O_2 is limiting on the pseudo-steady state conversion.

3.10. Insights into the active sites

To understand the selectivity changes upon reactivation, which are highest at the initial stage of the reaction, the active species concentration for this reaction (ketonic carbonyl C=O) [55] was assessed by the O*1s* XPS (Table 3, Fig. 9) on the fresh MWCNT and 15h-reactivated catalysts. The active site model is based on a quinone-to-hydroquinone redox mechanism, where the quinone abstract hydrogens from EB to form styrene, and O_2 would oxidize the hydroquinone back into quinone [46,50,56]. From the XPS data, the ketonic C=O concentration (ca. 530.6 eV) is slightly higher after reactivation (0.5 vs 0.3 at.%), but the values are within the limits of the standard deviation of both (Table 3). Hence, it cannot be claimed that these species are enhanced. However, the phenol C-OH groups (ca. 533.5 eV) are more pronouncedly enhanced (5.9 vs 2.3 at.%) with statistically meaningful standard deviations. Though C=O has been considered the sole active sites in carbons/coke-mediated EB-ODH, there are some arguments to consider the C-OH as active sites as well. First, it is likely that phenols oxidize during reaction forming ketonics and engage in the mechanism. Secondly, the active site interpretation should consider both ketonic and phenol groups since the mechanism operates as a redox pair C=O ↔ C-OH. The true pairs are those in a ´certain close proximity´ to activate the ethyl group, and such an amount remains difficult to assess. At least, for our catalytic data, the sum of both ketonic and phenol groups is a good qualitative descriptor of the active sites. The higher concentration of these species upon reactivation can explain the ST selectivity enhancement (i.e., the catalyst becomes more ST selective), and the derived EB conversion effect, which was explained by the model. Note that the reactivation-induced enhancement occurs at the beginning of the run without much coking. The decay with TOS can be cautiously attributed to coking side effects that deserve further study.

A comparison of the C=O and C-OH values in Table 3 (cf. raw two and three), shows that the reactivation created C=O at expense of the C-OH, which decreased. This provides additional evidence for the interconversion between C-OH into C=O species, as pointed out above as a phenomenon that may be occurring during the reaction.

3.11. Thermal stability considerations

It may be relevant to bring some prior work in relation to the thermal stability under oxidative conditions. Frank et al. [48] proposed the passivation of MWCNT with B_2O_3 or P_2O_5 to enhance the thermal stability under oxidative conditions. Similar effects were observed by Valero-Romero et al. on naturally-derived porous carbons by P [57] and Zarubina et al. on carbon/silica hybrids by P [40]. Such promotional effect can be useful here (in this reaction) when operating under ODH-coke free conditions. Our results are more positive about the oxidative thermal stability of the MWCNT, in the sense that an ODH-coked MWCNT survived the thermal oxidative reactivation. It appears that the ODH-coke acts as a protective barrier against the MWCNT surface oxidation and combustion during the reaction and reactivation. Hence, the modification of the MWCNT with additives (such as P and B) is not required as long as ODH-coke is deposited. However, our approach requires additional tests to verify how long the MWCNT can survive various reaction/reactivation cycles and compare it with other catalysts.

4. Conclusions

This study proved the feasibility of an *in situ* oxidative thermal reactivation of a fouled MWCNT-supported organocatalyst in the O_2-mediated styrene synthesis, where the organocatalyst is the *in situ* formed ODH-coke. The tests were carried out under industrially-relevant conditions resulting in improved conversion and selectivity. The fouled MWCNT-supported organocatalyst can be reactivated by controlled ODH-coke combustion, and it becomes more styrene-selective after reactivation. The reactivated catalyst system consisted

Table 3
Oxygen-based surface functional groups determined by XPS from the O*1s* lines. Spectra can be found in Fig. 9. The peak assignments were done according to the proposal given by Qi et al. [55].

Material	"C=O" at.% [a] (ca. 530.6 eV)	"O-C=O" at.% [b] (ca. 531.9 eV)	"C-OH" at.% [c] (ca. 533.5 eV)
Fresh MWCNT [d]	0.3 ± 0.1	1.8 ± 0.4	2.3 ± 0.6
After reaction	*below detection*	3.7 ± 0.7	6.9 ± 0.9
Reactivation 15 h	0.5 ± 0.2	4.3 ± 0.7	5.9 ± 0.4

[a] Ketonic carbonyl groups.
[b] Sum of carboxylic acid, anhydride, lactone, and ester groups.
[c] Phenol groups.
[d] A more accurate approach would be measuring the MWCNT after a few hours on stream to evaluate the ODH-coke. However, as the conversion and selectivity did not change much after starting the reaction, we assumed the active sites (C=O/C-OH) on the original MWCNT dominates the performance or are similar in concentration/nature to the ODH-coke.

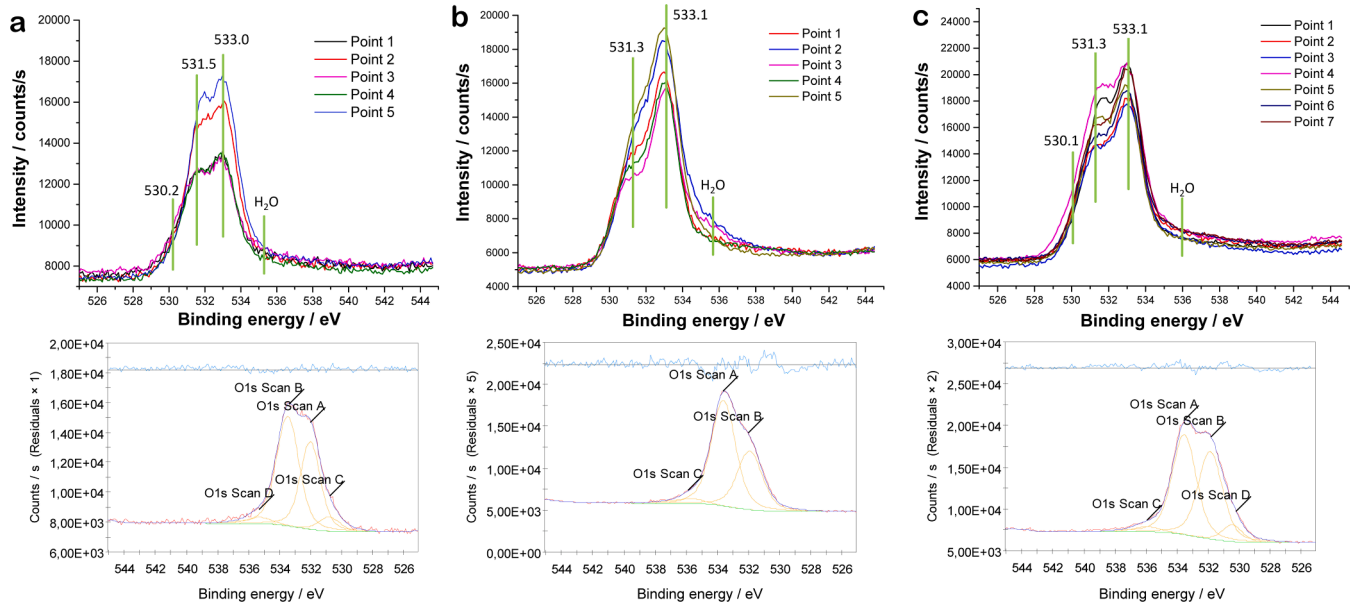

Fig. 9. XPS O*1s* spectra at different sample locations for (**a**) fresh MWCNT, (**b**) after reaction (1st) and (**c**) 15h-reactivated catalyst. Bottom shows an example for the deconvolution for each sample. The peak at ca. 535–536 eV is assigned to H_2O and was not quantified.

of the organocatalyst (unmodified and porous ODH-coke) and the MWCNT backbone. The initial improved selectivity after reactivation was explained by the increased concentration of surface ketonic and phenol groups, which act as active site pairs. The fact that the catalyst becomes more styrene selective explains the higher conversion to ethylbenzene. For this, a model was applied (via an O_2 mass balance assuming full conversion, which occurs in practice) which corroborated the experimental data. The model shows the dependency between EB conversion and selectivity during the whole run. This is important because it simplifies the number of root factors associated to the observed deactivation. The model explains: (i) the initially-improved parameters for the reactivated catalyst (higher ST selectivity gives rise to a higher EB conversion), and (ii) the course of the reaction with TOS where there is a link between conversion and selectivity; thus, the drop in EB conversion is associated to the higher CO_x selectivity for the reactivated catalyst (or lower to ST). Yet the model does not explain why the reactivated catalyst becomes less selective to styrene, or more to CO_x with TOS, which seems to be an unresolved topic. Overall, this study leads to three main messages: (a) survival of the MWCNT backbone after oxidative reactivation, (b) new organocatalyst formation (with positive features maintained for 20 h), and (c) a model explaining the relation between conversion and selectivity. The latter represents a paradigm shift in heterogeneous catalysis as they are normally considered independent parameters.

CRediT authorship contribution statement

Juan J. Mercadal: Investigation, Data curation, Methodology, Writing – review & editing. **Dmitrii Osadchii:** Investigation, Data curation, Writing – review & editing. **Valeriya Zarubina:** Methodology, Writing – review & editing. **María José Valero-Romero:** Writing – review & editing. **Ignacio Melián-Cabrera:** Conceptualization, Methodology, Data curation, Funding acquisition, Project administration, Resources, Supervision, Writing – original draft.

Declaration of Competing Interest

The authors declare that they have no known competing financial interests or personal relationships that could have appeared to influence the work reported in this paper.

Data availability

Data will be made available on request.

Acknowledgments

This work was supported by the Netherlands Organization for Scientific Research (NWO), under the Vidi Grant No. 10284 (www.nwo.nl/en/projects/10284), carried out at Groningen University and completed by I.M.C. at La Laguna University (www.ull.es). J.H. Marsman and L. Falco are thanked for assisting in the commissioning of the gas analysis system.

Supplementary materials

Supplementary material associated with this article can be found, in the online version, at doi:10.1016/j.mcat.2022.112525.

References

[1] J.D. Sachs, G. Schmidt-Traub, M. Mazzucato, D. Messner, N. Nakicenovic, J. Rockström, Six transformations to achieve the sustainable development goals, Nat. Sustain. 2 (2019) 805–814.
[2] T. Keijer, V. Bakker, J.C. Slootweg, Circular chemistry to enable a circular economy, Nat. Chem. 11 (2019) 190–195.
[3] M.F.L. De Volder, S.H. Tawfick, R.H. Baughman, A.J. Hart, Carbon nanotubes: present and future commercial applications, Science 339 (2013) 535–539.
[4] I. Melián-Cabrera, Catalytic materials: concepts to understand the pathway to implementation, Ind. Eng. Chem. Res. 60 (2021) 18545–18559.
[5] F. Rodriguez-Reinoso, The role of carbon materials in heterogeneous catalysis, Carbon 36 (1998) 159–175.
[6] A.A. Balandin, Thermal properties of graphene and nanostructured carbon materials, Nat. Mater. 10 (2011) 569–581.
[7] X. Liu, L. Dai, Carbon-based metal-free catalysts, Nat. Rev. Mater. 1 (2016) 16064.
[8] P. Serp, B. Machado, Nanostructured Carbon Materials for Catalysis, Royal Society of Chemistry, Cambridge, UK, 2015.
[9] M. Seredych, D. Hulicova-Jurcakova, G.Q. Lu, T.J. Bandosz, Surface functional groups of carbons and the effects of their chemical character, density and accessibility to ions on electrochemical performance, Carbon 46 (2008) 1475–1488.
[10] H.C. Foley, Carbogenic molecular sieves: synthesis, properties and applications, Microporous Mater. 4 (1995) 407–433.
[11] J. Zhang, X. Liu, R. Blume, A. Zhang, R. Schlögl, D.S. Su, Surface-modified carbon nanotubes catalyze oxidative dehydrogenation of *n*-butane, Science 322 (2008) 73–77.

[12] Y. Cao, B. Li, G. Zhong, Y. Li, H. Wang, H. Yu, F. Peng, Catalytic wet air oxidation of phenol over carbon nanotubes: synergistic effect of carboxyl groups and edge carbons, Carbon 133 (2018) 464–473.
[13] E. Lam, J.H.T. Luong, Carbon materials as catalyst supports and catalysts in the transformation of biomass to fuels and chemicals, ACS Catal. 4 (2014) 3393–3410.
[14] E.J. Askins, M.R. Zoric, M. Li, Z. Luo, K. Amine, K.D. Glusac, Toward a mechanistic understanding of electrocatalytic nanocarbon, Nat. Commun. 12 (2021) 3288.
[15] V. Zarubina, C. Nederlof, B. van der Linden, F. Kapteijn, H.J. Heeres, M. Makkee, I. Melián-Cabrera, Making coke a more efficient catalyst in the oxidative dehydrogenation of ethylbenzene using wide-pore transitional aluminas, J. Mol. Catal. A Chem. 381 (2014) 179–187.
[16] I. Melián-Cabrera, V. Zarubina, C. Nederlof, F. Kapteijn, M. Makkee, An *in situ* reactivation study reveals the supreme stability of γ-alumina for the oxidative dehydrogenation of ethylbenzene to styrene, Catal. Sci. Technol. 8 (2018) 3733–3736.
[17] H. Ba, G. Tuci, C. Evangelisti, M. Ceppatelli, L. Nguyen-Dinh, V. Dal Santo, F. Bossola, J.M. Nhut, A. Rossin, P. Granger, G. Giambastiani, C. Pham-Huu, Second youth of a metal-free dehydrogenation catalyst: when γ-Al_2O_3 meets coke under oxygen- and steam-free conditions, ACS Catal. 9 (2019) 9474–9484.
[18] S. Ott, A. Orfanidi, H. Schmies, B. Anke, H.N. Nong, J. Hübner, U. Gernert, M. Gliech, M. Lerch, P. Strasser, Ionomer distribution control in porous carbon-supported catalyst layers for high-power and low Pt-loaded proton exchange membrane fuel cells, Nat. Mater. 19 (2020) 77–85.
[19] M.B. Gawande, P. Fornasiero, R. Zboril, Carbon-based single-atom catalysts for advanced applications, ACS Catal. 10 (2020) 2231–2259.
[20] I.C. Gerber, P. Serp, A theory/experience description of support effects in carbon-supported catalysts, Chem. Rev. 120 (2020) 1250–1349.
[21] J.A. Moulijn, M. Makkee, A.E. van Diepen, Chemical Process Technology, 2nd ed., Wiley-VCH, Chichester, U.K., 2013, p. 56.
[22] R.A. Meyers, Handbook of Petrochemicals Production Processes, McGraw-Hill, New York, USA, 2005, pp. 11.1–11.34.
[23] F. Cavani, F. Trifiro, Alternative processes for the production of styrene, Appl. Catal. A 133 (1995) 219–239.
[24] V. Zarubina, H. Talebi, C. Nederlof, F. Kapteijn, M. Makkee, I. Melián-Cabrera, On the stability of conventional and nano-structured carbon-based catalysts in the oxidative dehydrogenation of ethylbenzene under industrially relevant conditions, Carbon 77 (2014) 329–340.
[25] G.C. Grunewald, R.S. Drago, Oxidative dehydrogenation of ethylbenzene to styrene over carbon-based catalysts, J. Mol. Catal. 58 (1990) 227–233.
[26] M.F.R. Pereira, J.J.M. Orfão, J.L. Figueiredo, Oxidative dehydrogenation of ethylbenzene on activated carbon catalysts. I. Influence of surface chemical groups, Appl. Catal. A Gen. 184 (1999) 153–160.
[27] N. Keller, N.I. Maksimova, V.V. Roddatis, M. Schur, G. Mestl, Y.V. Butenko, V. L. Kuznetsov, R. Schlögl, The catalytic use of onion-like carbon materials for styrene synthesis by oxidative dehydrogenation of ethylbenzene, Angew. Chem. Int. Ed. 41 (2002) 1885–1888.
[28] D.S. Su, N.I. Maksimova, G. Mestl, V.L. Kuznetsov, V. Keller, R. Schlögl, N. Keller, Oxidative dehydrogenation of ethylbenzene to styrene over ultra-dispersed diamond and onion-like carbon, Carbon 45 (2007) 2145–2151.
[29] G. Mestl, N.I. Maksimova, N. Keller, V.V. Roddatis, R. Schlögl, Carbon nanofilaments in heterogeneous catalysis: an industrial application for new carbon materials? Angew. Chem. Int. Ed. 40 (2001) 2066–2068.
[30] T.J. Zhao, W.Z. Sun, X.Y. Gu, M. Rønning, D. Chen, Y.C. Dai, W.K. Yuan, A. Holmen, Rational design of the carbon nanofiber catalysts for oxidative dehydrogenation of ethylbenzene, Appl. Catal. A Gen. 323 (2007) 135–146.
[31] J. Diao, Z. Feng, R. Huang, H. Liu, S. Bee, A. Hamid, D.S. Su, Selective and stable ethylbenzene dehydrogenation to styrene over nanodiamonds under oxygen-lean conditions, ChemSusChem 9 (2016) 662–666.
[32] L. Wang, J. Zhang, D.S. Su, Y. Ji, X. Cao, F.S. Xiao, Simple preparation of honeycomb-like macrostructured and microporous carbons with high performance in oxidative dehydrogenation of ethylbenzene, Chem. Mater. 19 (2007) 2894–2897.
[33] D.S. Su, J.J. Delgado, X. Liu, D. Wang, R. Schlögl, L. Wang, Z. Zhang, Z. Shan, F. S. Xiao, Highly ordered mesoporous carbon as catalyst for oxidative dehydrogenation of ethylbenzene to styrene, Chem. Asian J. 4 (2009) 1108–1113.
[34] L. Wang, J.J. Delgado, B. Frank, Z. Zhang, Z. Shan, D.S. Su, F.S. Xiao, Resin-derived hierarchical porous carbon spheres with high catalytic performance in the oxidative dehydrogenation of ethylbenzene, ChemSusChem 5 (2012) 687–693.
[35] M.F.R. Pereira, J.L. Figueiredo, J.J.M. Orfão, P. Serp, P. Kalck, Y. Kihn, Catalytic activity of carbon nanotubes in the oxidative dehydrogenation of ethylbenzene, Carbon 42 (2004) 2807–2813.
[36] J. Zhang, D.S. Su, A. Zhang, D. Wang, R. Schlögl, C. Hebert, Nanocarbon as robust catalyst: mechanistic insight into carbon-mediated catalysis, Angew. Chem. Int. Ed. 46 (2007) 7319–7323.
[37] C. Nederlof, V. Zarubina, I. Melián-Cabrera, H.J. Heeres, F. Kapteijn, M. Makkee, Application of staged O_2 feeding in the oxidative dehydrogenation of ethylbenzene to styrene over Al_2O_3 and P_2O_5/SiO_2 catalysts, Appl. Catal. A Gen. 476 (2014) 204–214.
[38] C. Nederlof, V. Zarubina, I. Melián-Cabrera, H.J. Heeres, F. Kapteijn, M. Makkee, Oxidative dehydrogenation of ethylbenzene to styrene over alumina: effect of calcination, Catal. Sci. Technol. 3 (2013) 519–526.
[39] C. Nederlof, P. Vijfhuizen, V. Zarubina, I. Melián-Cabrera, F. Kapteijn, M. Makkee, A TEOM investigation on coke formation in the oxidative dehydrogenation of ethylbenzene to styrene, Catal. Sci. Technol. 4 (2014) 3879–3890.
[40] V. Zarubina, H. Talebi, H. Jansma, K. Góra-Marek, C. Nederlof, F. Kapteijn, M. Makkee, I. Melián-Cabrera, On the thermal stabilization of carbon-supported SiO_2 catalysts by phosphorus: evaluation in the oxidative dehydrogenation of ethylbenzene to styrene and a comparison with relevant catalysts, Appl. Catal. A Gen. 514 (2016) 173–181.
[41] G.E. Vrieland, P.G. Menon, Nature of the catalytically active carbonaceous sites for the oxydehydrogenation of ethylbenzene to styrene: a brief review, Appl. Catal. 77 (1991) 1–8.
[42] A.E. Lisovskii, C. Aharoni, Carbonaceous deposits as catalysts for oxydehydrogenation of alkylbenzenes, Catal. Rev. Sci. Eng. 36 (1994) 25–74.
[43] M. Thommes, K. Kaneko, A.V. Neimark, J.P. Olivier, F. Rodriguez-Reinoso, J. Rouquerol, K.S.W. Sing, Physisorption of gases, with special reference to the evaluation of surface area and pore size distribution, Pure Appl. Chem. 87 (2015) 1051–1069.
[44] L. López Pérez, V. Zarubina, H.J. Heeres, I. Melián-Cabrera, Condensation-enhanced self-assembly as a route to high surface area α-aluminas, Chem. Mater. 25 (2013) 3971–3978.
[45] S. Tanuma, C.J. Powell, D.R. Penn, Calculations of electron inelastic mean free paths. V. Data for 14 organic compounds over the 50–2000 eV range, Surf. Interface Anal. 21 (1994) 165–176.
[46] I. Melián-Cabrera, V. Zarubina, Selectivity-induced conversion model explaining the coke-catalysed O_2-mediated styrene synthesis over wide-pore aluminas, Mol. Catal. 524 (2022), 112301.
[47] J.P. Tessonnier, D. Rosenthal, T.W. Hansen, C. Hess, M.E. Schuster, R. Blume, F. Girgsdies, N. Pfänder, O. Timpe, D.S. Su, R. Schlögl, Analysis of the structure and chemical properties of some commercial carbon nanostructures, Carbon 47 (2009) 1779–1798.
[48] B. Frank, A. Rinaldi, R. Blume, R. Schlögl, D.S. Su, Oxidation stability of multiwalled carbon nanotubes for catalytic applications, Chem. Mater. 22 (2010) 4462–4470.
[49] X. Sun, Y. Ding, B. Zhang, R. Huang, D. Chen, D.S. Su, Insight into the enhanced selectivity of phosphate-modified annealed nanodiamond for oxidative dehydrogenation reactions, ACS Catal. 5 (2015) 2436–2444.
[50] W. Qi, P. Yan, D.S. Su, Oxidative dehydrogenation on nanocarbon: insights into the reaction mechanism and kinetics via *in situ* experimental methods, Acc. Chem. Res. 51 (2018) 640–648.
[51] P.X. Hou, C. Liu, H.M. Cheng, Purification of carbon nanotubes, Carbon 46 (2008) 2003–2025.
[52] W. Kiciński, S. Dyjak, Transition metal impurities in carbon-based materials: pitfalls, artifacts and deleterious effects, Carbon 168 (2020) 748–845.
[53] M.F.R. Pereira, J.J.M. Órfão, J.L. Figueiredo, Oxidative dehydrogenation of ethylbenzene on activated carbon catalysts. 3. Catalyst deactivation, Appl. Catal. A Gen. 218 (2001) 307–318.
[54] M.F.R. Pereira, J.J.M. Órfão, J.L. Figueiredo, Oxidative dehydrogenation of ethylbenzene on activated carbon fibers, Carbon 40 (2002) 2393–2401.
[55] W. Qi, W. Liu, B. Zhang, X. Gu, X. Guo, D.S. Su, Oxidative dehydrogenation on nanocarbon: identification and quantification of active sites by chemical titration, Angew. Chem. Int. Ed. 52 (2013) 14224–14228.
[56] Y. Iwasawa, H. Nobe, S. Ogasawara, Reaction mechanism for styrene synthesis over polynaphthoquinone, J. Catal. 31 (1973) 444–449.
[57] M.J. Valero-Romero, F.J. García-Mateos, J. Rodríguez-Mirasol, T. Cordero, Role of surface phosphorus complexes on the oxidation of porous carbons, Fuel Process. Technol. 157 (2017) 116–126.